



# Delayed transition in a plane channel flow with high contraction ratio

S. Raghuram<sup>1</sup> · O. N. Ramesh<sup>1</sup>

Received: 7 January 2021 / Revised: 23 April 2021 / Accepted: 1 June 2021 / Published online: 16 June 2021  
© The Author(s), under exclusive licence to Springer-Verlag GmbH Germany, part of Springer Nature 2021

## Abstract

Large delay in the onset of laminar–turbulent transition and the protraction of its extent in a channel flow are achieved by connecting it to a wind tunnel with very high effective area contraction ratio ( $c$ ). Fully developed flow is established in the channel using a blower-based open-circuit wind tunnel, and 2D velocity field is measured using particle image velocimetry. The contractions are carefully designed with optimal parameters so as to have minimal non-uniformity at the exit, avoidance of boundary layer separation at the contraction inlet and exit and reduction in turbulence levels in the flow. This ultrahigh contraction ratio causes large reduction in the disturbance levels leading to delay in the onset of transition (at  $Re_m = 2050$  rather than the usual value of around 1500) and protraction of the extent of the transitional regime by around 4 times ( $\Delta Re_m = 3150$  as opposed to the usual value of around 800). Here  $Re_m = \frac{2u_m h}{\nu}$  is the bulk Reynolds number,  $u_m$  is the bulk velocity,  $h$  the channel half height and  $\nu$  the kinematic viscosity. This is confirmed by the values of the centerline turbulence intensity obtained around the onset of transition from current measurements, which are found to be lower than those from other studies in the literature with lower values of  $c$ .

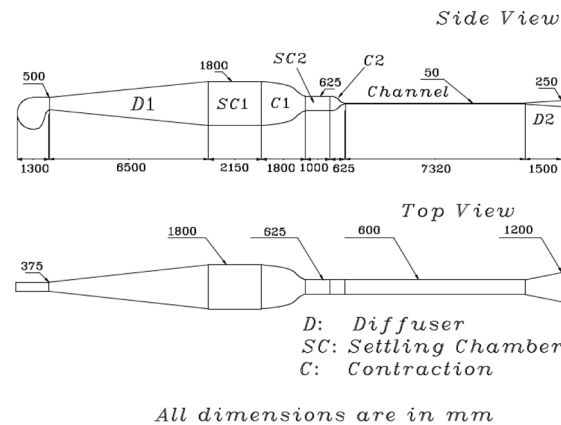
---

✉ O. N. Ramesh  
onr@iisc.ac.in

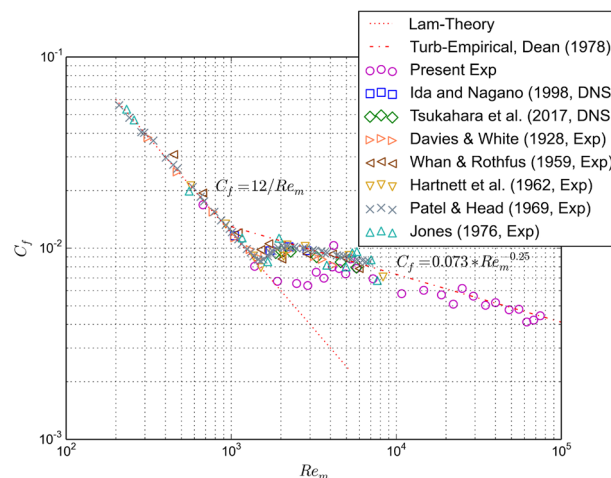
<sup>1</sup> Department of Aerospace Engineering, Indian Institute of Science, Bangalore 560012, India

## Graphic abstract

## Schematic of a Channel Wind Tunnel with Ultra High Contraction Area Ratio



## Coefficient of friction measured in the channel



## 1 Introduction

Transition control and drag reduction in plane channel flow has been studied by many investigators for wall-bounded flows in the past. Various strategies have been employed toward this such as using hydrophobic wall (Nouri et al. 2012), infusing a lubricant within microgrooves made on the surface (Chang et al. 2019), polymer additives (Min et al. 2003b; Ptasiniski et al. 2003; Dimitropoulos et al. 1998; Li et al. 2006; Sureshkumar et al. 1997), suspension of solid particles (Niazi Ardekani et al. 2017), flow induced by a traveling wave (Min et al. 2006; Tomiyama and Fukagata 2013), by application of Magnetohydrodynamic (MHD) Lorentz force (Min et al. 2003a; Breuer et al. 2004), using

Dielectric Barrier Discharge (DBD) plasma actuator (Mahfoze and Laizet 2017), large eddy breakup (LEBU) devices or blade manipulators (Vasudevan et al. 1992), active feedback control using blowing and suction (Lee et al. 1997; Marusic et al. 2007). While the above methods focus on altering the fluid properties, boundary conditions or the flow within the channel, a few studies have investigated the effect of level of oncoming free stream turbulence (FST) on transition control. It is established (Downs and White 2013; Ovchinnikov et al. 2008) that the level of FST has a profound impact on the rate of growth of disturbances (the mechanism involved in transition) and hence can lead to the delay or advancement of transition. Various passive turbulence manipulators such as screens, perforated plates, porous

foams and honeycombs have been studied in Loehrke and Nagib (1972). The study shows the efficacy of these manipulators in reducing free stream turbulence, using hot-wire anemometry and hydrogen-bubble visualization techniques.

For plane channel flow (or a pipe flow), the transition characteristics are dictated by the shape of the velocity profile, disturbance levels at the entrance to the channel flow. It is also observed that small variations in the entrance velocity profile due to the geometry impacts the extent of the laminar region and the  $Re_m$  corresponding to the onset of transition (Tritton 1977). Another way of reducing free stream turbulence is presumably by increasing the contraction ratio ( $c$ ) (Ramjee et al. 1972; Derbunovich et al. 1987; Reif et al. 2005). A simple vortex dynamics argument leads to the view that, in a contraction with area ratio  $c$ , while the longitudinal component of velocity fluctuation reduces by  $c$  the lateral components increase by  $\sqrt{c}$  (Prandtl 1933; Uberoi 1956; Tennekes and Lumley 1972; Mehta 1979). Also the flow non-uniformities decrease by a factor of  $c^2$  in the stream-wise direction (Prandtl 1933; Corrsin 1952; Mehta 1979). The effect of using contractions with high area ratio toward delaying transition in plane channel flows does not seem to have been investigated in the past and this will be the focus of the present study. Disturbance levels before the entrance region to the channel is sought to be reduced, since the  $Re_m$  is constrained to be constant along the channel. Toward this, we use the upstream part of the system to be a part from a blower wind tunnel that has a contraction with  $c = 8.3$  to be combined with a further contraction with  $c = 13$ , resulting in an effective contraction of area ratio  $c = 108$ . Effectively, the high contraction ratio resulted in delay in the onset of transition to  $Re_m \approx 2050$  compared to the standard value of  $Re_m \approx 1500$  as stated in the literature. Furthermore, the transition process was completed at  $Re_m = 5200$ , resulting in protraction of the transition regime.

The paper is organized as follows: The details of the overall channel tunnel construction, design of subsystems such as the contraction and diffuser, detailed pressure loss calculations for various parts of the channel along with the blower selection are presented in Sect. 2. Methods used to measure the mean velocity and skin friction are described in Sect. 3. The main results substantiating the delay in transition are presented in Sect. 4. Finally, some concluding remarks are presented in Sect. 5.

## 2 The channel tunnel (chunnel)

An existing blower wind tunnel, wherein the sections downstream of the contraction section are removed, is used as the upstream section. This is followed by a downstream plane channel starting with its own settling chamber and a contraction section. The plane channel section

is followed by a diffuser. This combination of tunnel and channel (Chunnel) was designed such that the effective  $c$  is very large—the original contraction ratio of 8.3 of the wind tunnel is augmented by the contraction ratio of 13 of the channel section making an effective ratio of about 108. The purpose of building this chunnel is to get a relatively quiet channel flow where both transitional and turbulent plane channel flows can be studied in a comprehensive fashion. Figure 1 shows the design drawing of the chunnel. A centrifugal blower and an a.c. motor with maximum power rating of 55 hp is used to drive the flow. A diffuser (D) connects the blower to a settling chamber (SC1) with a honeycomb to straighten the flow, followed by the first contraction (C1). One more contraction (C2) is designed and is connected to C1 by a constant area section (SC2).

A two-dimensional channel of cross-sectional area ratio,  $AR = 12$  and of length  $L/(2h) = 146$  have been designed. Similar designs were used by Zanon (2003) ( $AR = 12, L/(2h) = 115$ ), Monty and Chong (2009) ( $AR = 11.7, L/(2h) = 205$ ). Based on this, the channel dimensions were chosen to be 7320 mm  $\times$  600 mm  $\times$  50 mm, also to ensure reasonable resolution of measurements within the constraint of lab space available. The channel is connected to the exit of the second contraction.

A contraction is designed to smoothly take the flow from the exit of SC2 to the entrance of the channel. The contraction design objectives are minimal non-uniformity at exit, avoidance of boundary layer separation, reduction of relative turbulence level, least pressure loss, cost and available space (Morel 1977; Ramaseshan and Ramaswamy 2002). The geometric parameters that affect these considerations are area contraction ratio ( $c$ ), length of the contraction and the shape of the contraction contour (Morel 1975). The final expression for the contraction based on Ramaseshan and Ramaswamy (2002); Borger (1976) is

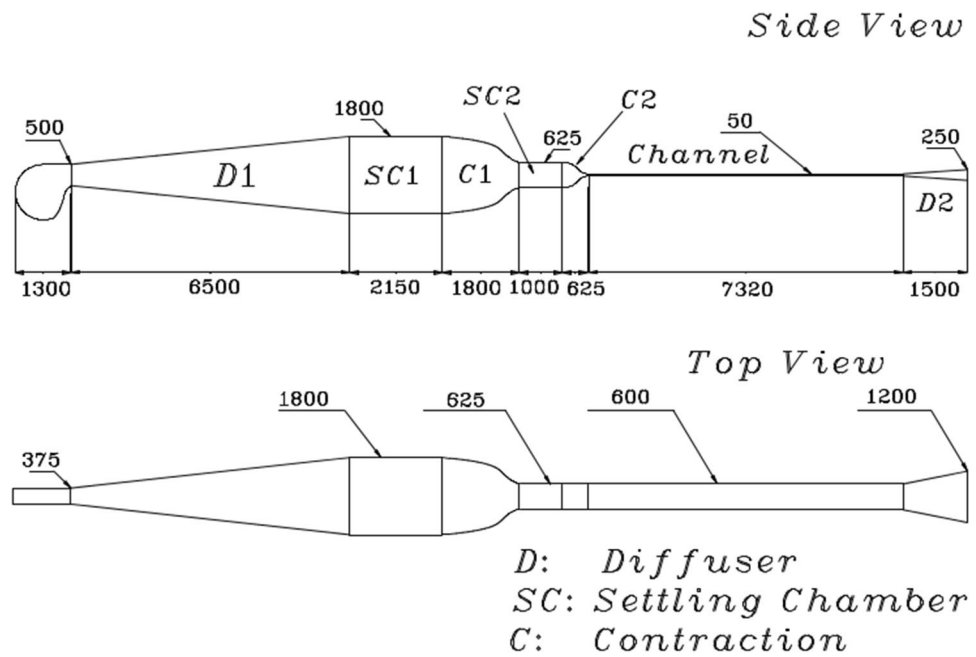
$$\eta = 6\xi^5 - 15\xi^4 + 10\xi^3 \quad (1)$$

where  $\xi = \frac{x}{L}$  and  $\eta = \frac{y-y_i}{y_o-y_i}$ . In our case,  $y_i = 312.5$  mm,  $y_o = 25$  mm and  $L = 625$  mm for the longitudinal contraction. For static pressure recovery, an exit diffuser of exit dimensions 1200 mm  $\times$  250 mm and length 1.5 m is used.

## 3 Measurements in the transition regime

The channel flow experiments were performed in the open-circuit blower-type wind tunnel as described in Sect. 2. All measurements are made at the channel test section located around 6000 mm from the entrance. For a plane channel, the mean momentum equation when simplified leads to

**Fig. 1** Channel tunnel design drawing



All dimensions are in mm

$$\frac{h}{\rho} \left( \frac{-dP_0}{dx} \right) = u_\tau^2 = \frac{\tau_w}{\rho} = \nu \left( \frac{du}{dy} \right)_w \quad (2)$$

Hence, the wall shear stress  $\tau_w$  and friction velocity  $u_\tau$  are calculated directly from static pressure measured along the streamwise direction.

Pressure is measured using a micromanometer from Furness Controls FCO 510. Two units of FCO 510 capable of measuring pressure difference in different ranges 0–200 mmH<sub>2</sub>O (0–18 m/s) and 0–2000 mmH<sub>2</sub>O (0–57 m/s) were used. The first manometer has precision to 3 decimals and is used for measuring in the transitional flow regime since it involves low pressure differences and is thus very sensitive. The second manometer has precision to 2 decimals is sufficient for measurements in the turbulent regime. The manometer is set to the desired time of acquisition (sampling rate is 1 Hz), and the data are by acquired using FC487 software provided by Furness Controls. For all the cases considered, pressure data are averaged for 1 min (acquired for 2 mins, out of which the first 1 min is used for settling down and not considered in the averaging).

The accuracy of wall shear stress measurement is critical in wall-bounded turbulence, since all the scaling results are largely dependent on this. Zanon (2003) established that the shear stress obtained using static pressure measurements are fairly accurate and compare well with values obtained from oil-film interferometry. Hence, static pressure measurements are carried out to obtain wall shear stress. A recent study that measures wall shear stress in a transitional plane

channel flow using hot film sensors has been reported by Agrawal et al. (2008).

There are 50 static pressure ports installed on the bottom wall of the channel with a diameter of 0.5 mm and pitch of 3cm. The static pressure (streamwise) gradient ( $dP_w/dx$ ) is calculated as the slope of linear fit to the wall pressure plotted against streamwise distance. Friction velocity ( $u_\tau$ ) is then calculated from the streamwise pressure gradient using Eq. 2. Figure 2 shows the pressure drop plotted against streamwise distance for various  $Re_m$  in the range 2492–5276.

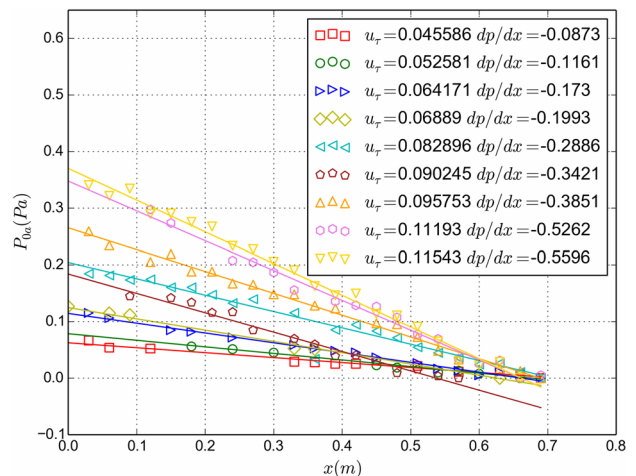


**Fig. 2** Calculation of friction velocity using wall pressure measurements along the streamwise direction for various speeds

The pressure gradient is thus calculated as the slope of the fitted straight line as shown in Fig. 2. The friction Reynolds number (Karman number) is calculated as  $Re_\tau = u_\tau h/\nu$  and the wall shear stress as  $\tau_w = \rho u_\tau^2$ . It is found that for the lowest possible motor RPM of the tunnel,  $Re_m$  is calculated to be 5760, which corresponds possibly to fully developed turbulence and lower flow rates are required to establish flow in the transitional regime. In order to achieve this, a constant area section (of length around 0.2 m) used to connect the exit of the blower to the first diffuser is removed to bleed the flow and reduce the mass flow rate. This leads to a portion of the oncoming flow lost to the atmosphere, thus reducing the flow rate of the flow entering the tunnel. With this arrangement, measurements could be performed from the end of the laminar regime through the complete transitional regime and beginning of turbulent regime till  $Re_m$  of 5760.

Two-dimensionality of the flow is checked at the entrance to the channel (contraction exit). One of the main causes for non-uniformity is the curvature of the streamlines when the flow passes through the contraction. As the flow enters the channel, there would be a convex curvature of the streamlines from the contraction away from the wall, toward the center, and the centripetal effects are balanced by the pressure gradient (In this connection please see Panton (2013) and Fig. 7.2 therein showing the entrance velocity profile and its associated discussion).

Figure 3 shows static pressure measurements right at the entrance for a range of tunnel operating speeds (based on Reynolds number at the centerline and channel half height). For each speed, as we move away from the center, toward the side walls, static pressure is nearly a constant up to 30% about the centerline. Somewhere around 60% from the centerline, it reaches a maximum and starts decreasing again, indicating the curvature effects are prominent around 60%.

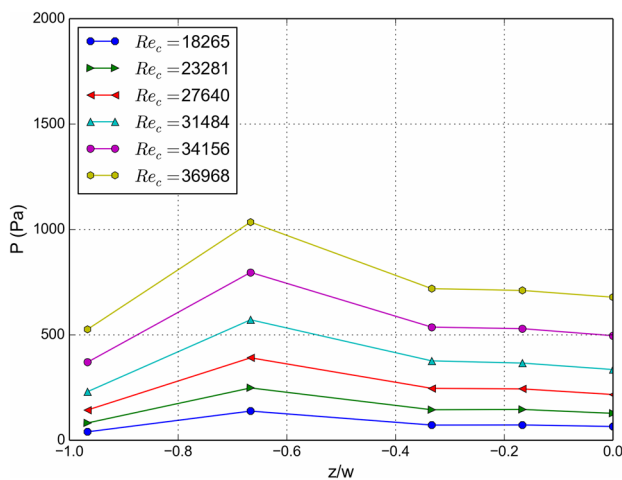


Fig. 3 Static pressure measured at the channel entrance with spanwise distance for various speeds

For the highest speed case considered, the static pressure differs by 4.7%, 5.7%, 52.5% and -22.5% from the centerline value at distances  $w/6$ ,  $w/3$ ,  $2w/3$  and  $29w/30$  from the centerline. This indicates that the curvature effects due to the contraction are prominent away from the center and the central region of the channel is fairly two-dimensional even at the entrance, presumably because of the reduced non-uniformity caused by the high contraction ratio.

Two-dimensional velocity field is measured in the x-y plane using LaVision FlowMaster particle image velocimetry (PIV) system is used with repetition rate of 15 Hz. From the PIV measurements, first- and second-order statistics were evaluated for various averaging times (30 s, 40 s, 50 s, 60 s). While the first-order statistics converge much earlier, the second-order statistics converge only around 50s averaging time (Figs. 4, 5). Hence, 1 min (900 snapshots) is taken as the acquisition time

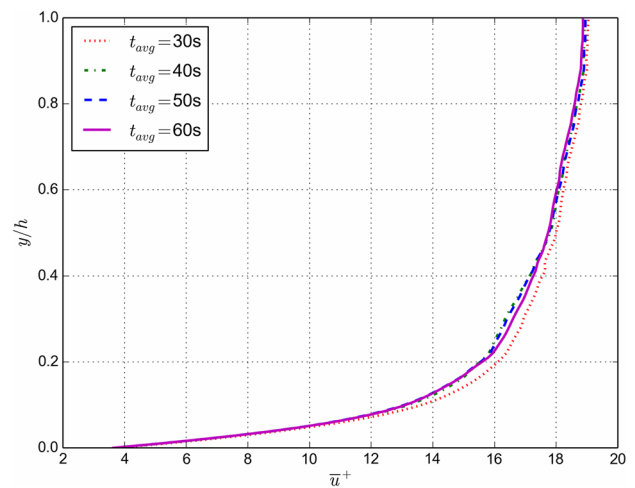


Fig. 4 U profiles plotted for various averaging times for  $Re_m = 4100$

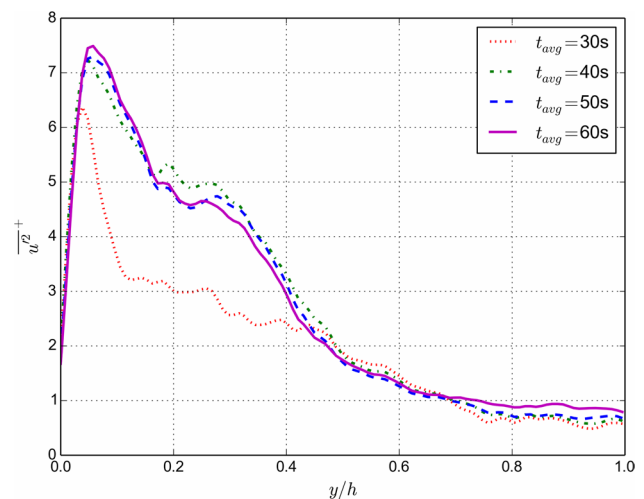
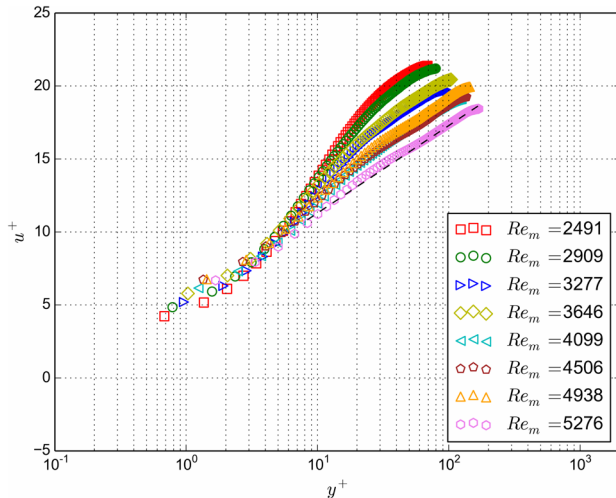


Fig. 5  $\overline{u^2}$  profiles plotted for various averaging times for  $Re_m = 4100$

**Table 1** Summary of experimental parameters

Measurement method	Instrument details	Quantities measured	Sampling rate	Total duration (s)	$Re_m$ range
Micromanometer	Furness controls FCO 510	$P$ (static and total)	1 Hz	1 min	2500–80,000
PIV	LaVision GmbH	$u, v$ along $x$ - $y$ plane	15 Hz	1 min	2500–80,000



**Fig. 6** Mean velocity profiles for various  $Re_m$  cases

for all the speeds considered. Summary of the experimental parameters is tabulated in Table 1.

Figure 6 shows the mean velocity profile obtained from the PIV measurements for various transitional  $Re_m$ , plotted in the semilog scale. It will be seen from the  $C_f$  curve later that the last case  $Re_m = 5276$  correspond to the fully developed turbulent regime. The variance of streamwise velocity fluctuations is also plotted for the same set of  $Re_m$  in Fig. 7. It can be seen that the normalized intensity comes down with  $Re_m$  presumably due to increase in value of  $u_\tau$ .

### 4 Delayed transition

The skin friction coefficient,  $C_f$  is determined as the ratio of wall shear stress to mean dynamic pressure.

$$C_f = \frac{\tau_w}{\frac{1}{2}\rho u_m^2} = 2 \left( \frac{u_\tau}{u_m} \right)^2 \quad (3)$$

This is calculated using  $u_\tau$  (estimated from the wall pressure gradient) and  $u_m$  (obtained from the PIV measurements) as described in Sect. 3. This is also done for few laminar and turbulent  $Re_m$  cases and the results are plotted in Fig. 8 against  $Re_m$  in the log–log scale.

Also plotted are lines corresponding to skin friction variation with  $Re_m$  for laminar [ $C_f = 12/Re_m$  from theory (White 1991)] and turbulent [empirical correlation (Dean

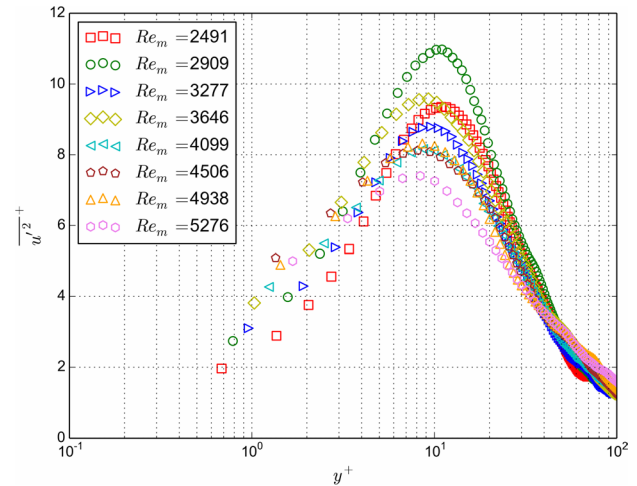


**Fig. 7** Variance profiles of streamwise velocity fluctuations for various  $Re_m$  cases

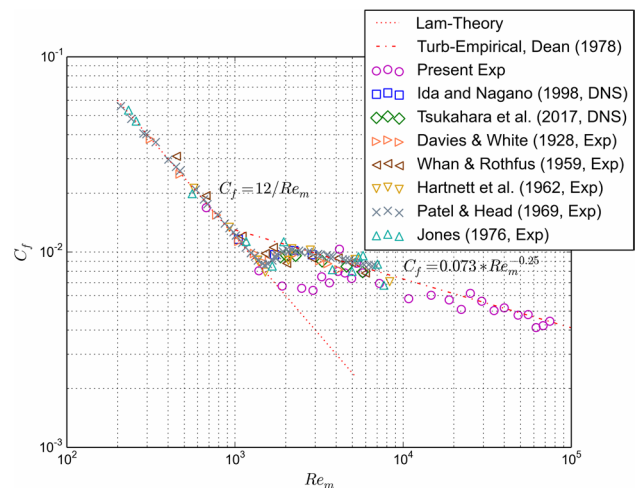


**Fig. 8** Skin friction coefficient variation with  $Re_m$

1978)] channel flow. The first two points in Fig. 8 that fall on the turbulent correlation line correspond to the case with  $Re_m = 5276$  as observed earlier in Fig. 6. There are a few experimental works (Davies and White 1928; Whan and Rothfus 1959; Hartnett et al. 1962; Patel and Head 1969; Jones 1976) and DNS works (Iida and Nagano 1998; Tsukahara et al. 2005) that report skin friction data in the transitional regime of channel flow. These are plotted along with the present data in Fig. 8. It is observed that the data

from present experiments are distinctly away from data of others around the transitional region. The data from other works show start of transition at  $Re_m$  of 1300 and end around 2100–2500 with the transition extent,  $\Delta Re_m \approx 1000$ , whereas data from present experiments show start of transition at 2050, ending at around 5200 with  $\Delta Re_m \approx 3150$  (summarized in Table 2). This is a relatively large delay in onset and also further protraction in the extent of the transitional regime. The mean velocity, non-dimensionalized in outer coordinates, at  $Re_m$  when the flow has departed from the laminar state, is plotted for the present study and compared with corresponding results from some other studies in the literature. The velocity profiles from other studies plotted around  $Re_m$  1500 just after transition onset value deviate from the laminar parabolic curve and fuller, thereby indicating that they are already transitional. In contrast, the profile from the present PIV measurements at  $Re_m \approx 1906$ , shown in Fig. 9, still follows the parabolic curve, showing it is still laminar, consistent with the observations from the  $C_f$  curve shown in Fig. 8.

A measure of the turbulence level in the fully developed channel section can be taken to be  $u'_{cl}/U_{cl}$ . This is indicated in 2 along with the onset and terminal Reynolds numbers as well as the experiments of others in the literature. The delayed onset and protracted transition zone of the present experiments are evident and correlated with the disturbance level in the centerline in the fully developed flow region. Figure 10 shows the turbulence intensity at the centerline from current experiments along with hot-wire measurements of Seki and Matsubara (2012) which had a contraction,  $c = 34$ —around 3 times smaller compared to the present experiments. The turbulence intensity of Seki and Matsubara (2012) at  $Re_m = 1530$  just after the start of transition is larger at 0.105, whereas corresponding value from the present experiments ( $Re_m \approx 2000$ ) is 0.067. This indicates the relative quietness of the flow presumably brought about by the larger contraction ratio in the present study. Furthermore, this also results in protracting the transition regime as can be seen in Fig. 10.

### 4.1 Mechanism causing transition onset delay

Turbulence in a pipe or a channel in the entrance region is generated in localized packets (turbulent slugs) close to the wall known. They are localized in streamwise and spanwise

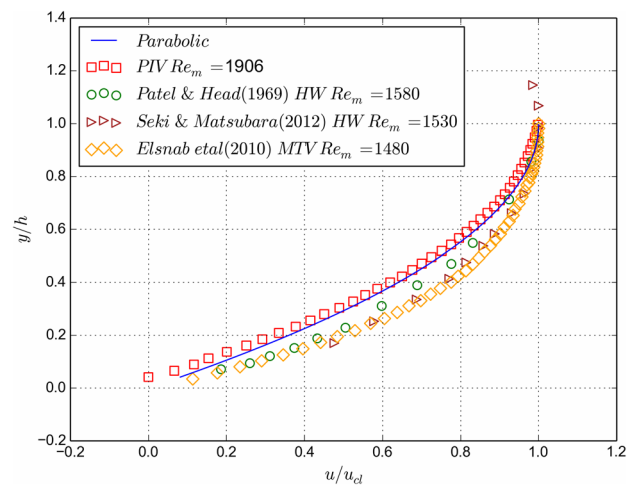


Fig. 9 Mean velocity profile plotted in outer coordinates compared with those from other experiments from literature around the start of transition

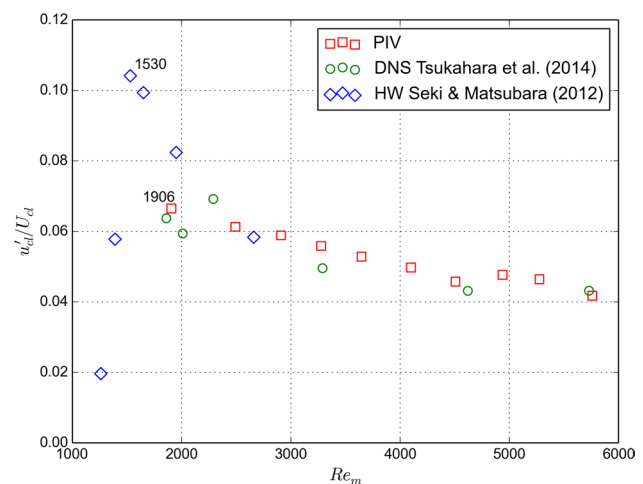


Fig. 10 Centerline turbulence intensity plotted with  $Re_m$  for present experiments as well as for those from literature

directions but spread quickly over the wall-normal direction (Wynanski and Champagne 1973). These slugs interact with each other and grow in size, while new slugs also originate with time. At some particular downstream distance, the slugs grow and spread through the domain making it completely turbulent. The critical  $Re$  at which the transition onset ensues is extremely sensitive to the geometry of entry

**Table 2** Transitional regime  $Re_m$  range and corresponding centerline turbulence intensities, comparison with others experimental values

Transitional regime	Current experiments			Others experiments		
	$Re_m$	$Re_\tau$	$u'_{cl}/U_{cl}$ (at $Re_m$ )	$Re_m$	$Re_\tau$	$u'_{cl}/U_{cl}$ (at $Re_m$ ) (Seki and Matsubara 2012)
Onset	2050	60	0.066 (1907)	1500	46	0.140 (1530)
End	5200	175	0.046 (5276)	2100–2500	60–70	0.042 (2660)

and the disturbance levels in the oncoming fluid (Tritton 1977). The entry flow depends on the geometries leading to the entrance, and is mostly irrotational. Boundary layer grows on both the walls and the velocity profile gets closer to parabolic shape as the boundary layers merge. When the boundary layer thickness is small compared to channel half width, flow is more prone to be unstable at high  $Re$  (Garg 1981; Sarpkaya 1975). Stable and unstable regions alternate with each other as the profile approaches Poiseuille flow. Amplification of disturbances in the unstable region could lead to onset of transition. The onset of transition is thus subjected to high variability. This is based on velocity profile at entrance having variations due to the entrance geometry that might affect the extent of unstable region; if there are sharp edges or corners, the disturbances would be amplified rapidly, leading to accelerated onset of transition.

The experimentally observed value of critical  $Re$  for plane channel flow is 1000–1100 (Biau 2008), while linear stability analysis shows a critical  $Re$  for transition to turbulence to be 5772 (Drazin and Reid 1981), showing subcritical nature of the instability (non-modal growth). Beyond the development length,  $Re$  is not a function of streamwise distance. This would mean the disturbance levels at the channel entrance plays a pivotal role in the delay or advancement of transition onset. The flow non-uniformities decrease by a factor of  $c^2$  in the streamwise direction where  $c$  is the contraction ratio (Prandtl 1933; Corrsin 1952; Mehta 1979). This causes a stabilizing influence with very low disturbance levels in the flow at the channel entrance. This would make the velocity profile more uniform and fuller (low shape factor) and the local Reynolds number (based on displacement thickness,  $\delta^*$  or momentum thickness,  $\theta$ ) in the entrance region would decrease. According to Drazin and Reid (1981), the critical  $Re$  for a boundary layer is a decreasing function of shape factor. The critical  $Re$  required for transition thus increases with flatter profiles resulting in delay in the onset of transition.

## 5 Conclusions

Fully developed transitional channel flow has been studied experimentally. A large contraction ratio of  $c = 108$ , brought about by combining in series two contractions was used. For this purpose, an existing blower wind tunnel was used as the upstream section, connected to a downstream channel. The aim of this study was to delay transition by increasing the contraction ratio as well as carefully designing the contraction geometry, thereby quietening the inflow to the channel. This resulted in a channel flow where the transition onset occurs at  $Re_m = 2050$  and transition was complete at  $Re_m = 5200$ . This is protracted compared to other results in

the literature which are typically about  $Re_m = 1500$ – $2300$ . In summary, effectively high contraction ratio delays transition onset and also protracts the extent of the transition region.

**Acknowledgements** ONR would like to acknowledge discussions with Prof. Tom Mullin (University of Oxford).

## References

- Agrawal R, Ng HC, Dennis DJ, Poole RJ (2020) Investigating channel flow using wall shear stress signals at transitional Reynolds numbers. *Int J Heat Fluid Flow*. <https://doi.org/10.1016/j.ijheatfluidflow.2019.108525>
- Biau D (2008) Linear stability of channel entrance flow. *Eur J Mech B/Fluids*. <https://doi.org/10.1016/j.euromechflu.2007.11.004>
- Borger GG (1976) The optimization of wind tunnel contractions for the subsonic range. NASA technical translation. National Aeronautics and Space Administration <https://books.google.com/books?id=qRvqGwAACAAJ>
- Breuer KS, Park J, Henoch C (2004) Actuation and control of a turbulent channel flow using Lorentz forces. *Phys Fluids*. <https://doi.org/10.1063/1.1647142>
- Chang J, Jung T, Choi H, Kim J (2019) Predictions of the effective slip length and drag reduction with a lubricated micro-groove surface in a turbulent channel flow. *J Fluid Mech*. <https://doi.org/10.1017/jfm.2019.468>
- Corrsin S (1952) Effect of wind-tunnel nozzle on steady-flow nonuniformities. *J Aeronaut Sci*. <https://doi.org/10.2514/8.2181>
- Davies CM, White SJ (1928) An experimental study of the flow of water in pipes of rectangular section. *Proc R Soc Lond Ser A Contain Pap Math Phys Character*. <https://doi.org/10.1098/rspa.1928.0086>
- Dean RB (1978) Reynolds number dependence of skin friction and other bulk flow variables in two-dimensional rectangular duct flow. *J Fluids Eng Trans ASME*. <https://doi.org/10.1115/1.3448633>
- Derbunovich GI, Zemskaya AS, Repik EU, Sosedko YP (1987) Effect of flow contraction on the level of turbulence. *Fluid Dyn*. <https://doi.org/10.1007/BF01052265>
- Dimitropoulos CD, Sureshkumar R, Beris AN (1998) Direct numerical simulation of viscoelastic turbulent channel flow exhibiting drag reduction: effect of the variation of rheological parameters. *J Non-Newton Fluid Mech*. [https://doi.org/10.1016/S0377-0257\(98\)00115-3](https://doi.org/10.1016/S0377-0257(98)00115-3)
- Downs RS, White EB (2013) Free-stream turbulence and the development of cross-flow disturbances. *J Fluid Mech*. <https://doi.org/10.1017/jfm.2013.484>
- Drazin PG, Reid WH (1981) Hydrodynamic stability
- Garg VK (1981) Stability of developing flow in a pipe: non-axisymmetric disturbances. *J Fluid Mech*. <https://doi.org/10.1017/S0022112081000694>
- Hartnett JP, Koh JC, McComas ST (1962) A comparison of predicted and measured friction factors for turbulent flow through rectangular ducts. *J Heat Transf*. <https://doi.org/10.1115/1.3684299>
- Iida O, Nagano Y (1998) Relaminarization mechanisms of turbulent channel flow at low Reynolds numbers. *Flow Turbul Combust*. <https://doi.org/10.1023/A:1009999606355>
- Jones OG (1976) An improvement in the calculation of turbulent friction in rectangular ducts. *J Fluids Eng Trans ASME*. <https://doi.org/10.1115/1.3448250>
- Lee C, Kim J, Babcock D, Goodman R (1997) Application of neural networks to turbulence control for drag reduction. *Phys Fluids*. <https://doi.org/10.1063/1.869290>



- Li CF, Gupta VK, Sureshkumar R, Khomami B (2006) Turbulent channel flow of dilute polymeric solutions: drag reduction scaling and an eddy viscosity model. *J Non-Newton Fluid Mech.* <https://doi.org/10.1016/j.jnnfm.2006.04.012>
- Loehrke RI, Nagib HM (1972) Experiments on management of free-stream turbulence. Technical rep, North Atlantic Treaty Organization, Chicago, Illinois
- Mahfoze O, Laizet S (2017) Skin-friction drag reduction in a channel flow with streamwise-aligned plasma actuators. *Int J Heat Fluid Flow.* <https://doi.org/10.1016/j.ijheatfluidflow.2017.05.013>
- Marusic I, Joseph DD, Mahesh K (2007) Laminar and turbulent comparisons for channel flow and flow control. *J Fluid Mech.* <https://doi.org/10.1017/S0022112006003247>
- Mehta RD (1979) The aerodynamic design of blower tunnels with wide-angle diffusers. *Prog Aerosp Sci.* [https://doi.org/10.1016/0376-0421\(77\)90003-3](https://doi.org/10.1016/0376-0421(77)90003-3)
- Min T, Choi H, Yoo JY (2003a) Maximum drag reduction in a turbulent channel flow by polymer additives. *J Fluid Mech.* <https://doi.org/10.1017/S0022112003005597>
- Min T, Yoo JY, Choi H, Joseph DD (2003b) Drag reduction by polymer additives in a turbulent channel flow. *J Fluid Mech.* <https://doi.org/10.1017/S0022112003004610>
- Min T, Kang SM, Speyer JL, Kim J (2006) Sustained sub-laminar drag in a fully developed channel flow. *J Fluid Mech.* <https://doi.org/10.1017/S0022112006000206>
- Monty JP, Chong MS (2009) Turbulent channel flow: comparison of streamwise velocity data from experiments and direct numerical simulation. *J Fluid Mech.* <https://doi.org/10.1017/S0022112009007769>
- Morel T (1975) Comprehensive design of axisymmetric wind tunnel contractions. *J Fluids Eng Trans ASME.* <https://doi.org/10.1115/1.3447255>
- Morel T (1977) Design of two-dimensional wind tunnel contractions. *J Fluids Eng Trans ASME.* <https://doi.org/10.1115/1.3448764>
- Niazi Ardekani M, Costa P, Breugem WP, Picano F, Brandt L (2017) Drag reduction in turbulent channel flow laden with finite-size oblate spheroids. *J Fluid Mech* 1607:00679. <https://doi.org/10.1017/jfm.2017.68>
- Nouri NM, Sekhvat S, Mofidi A (2012) Drag reduction in a turbulent channel flow with hydrophobic wall. *J Hydrodyn.* [https://doi.org/10.1016/S1001-6058\(11\)60267-9](https://doi.org/10.1016/S1001-6058(11)60267-9)
- Ovchinnikov V, Choudhari MM, Piomelli U (2008) Numerical simulations of boundary-layer bypass transition due to high-amplitude free-stream turbulence. *J Fluid Mech.* <https://doi.org/10.1017/S0022112008003017>
- Panton RL (2013) *Incompressible flow*, 4th edn
- Patel VC, Head MR (1969) Some observations on skin friction and velocity profiles in fully developed pipe and channel flows. *J Fluid Mech.* <https://doi.org/10.1017/S0022112069000115>
- Prandtl L (1933) Attaining a steady air stream in wind tunnels. Technical Memorandum National Advisory Committee For Aeronautics
- Ptasinski PK, Boersma BJ, Nieuwstadt FT, Hulsen MA, Van den Brule HA, Hunt JC (2003) Turbulent channel flow near maximum drag reduction: simulations, experiments and mechanisms. *J Fluid Mech.* <https://doi.org/10.1017/S0022112003005305>
- Ramaseshan S, Ramaswamy MA (2002) A rational method to choose optimum design for two-dimensional contractions. *J Fluids Eng Trans ASME.* <https://doi.org/10.1115/1.1456463>
- Ramjee V, Badri Narayanan MA, Narasimha R (1972) Effect of contraction on turbulent channel flow. *Zeitschrift für angewandte Mathematik und Physik ZAMP.* <https://doi.org/10.1007/BF01593207>
- Reif BAP, George WK, Hjärne J (2005) Effect of a contraction on turbulence. Part 2: theory. In: 43rd AIAA aerospace sciences meeting and exhibit - meeting papers. <https://doi.org/10.2514/6.2005-1120>
- Sarpkaya T (1975) An inviscid model of two-dimensional vortex shedding for transient and asymptotically steady separated flow over an inclined plate. *J Fluid Mech.* <https://doi.org/10.1017/S0022112075000717>
- Seki D, Matsubara M (2012) Experimental investigation of relaminarizing and transitional channel flows. *Phys Fluids.* <https://doi.org/10.1063/1.4772065>
- Sureshkumar R, Beris AN, Handler RA (1997) Direct numerical simulation of the turbulent channel flow of a polymer solution. *Phys Fluids.* <https://doi.org/10.1063/1.869229>
- Tennekes H, Lumley JL (1972) *A first course in turbulence*. The MIT Press, Boston
- Tomiyama N, Fukagata K (2013) Direct numerical simulation of drag reduction in a turbulent channel flow using spanwise traveling wave-like wall deformation. *Phys Fluids.* <https://doi.org/10.1063/1.4826887>
- Tritton DJ (1977) *Physical fluid dynamics*. *Phys Bull.* <https://doi.org/10.1088/0031-9112/28/9/048>
- Tsukahara T, Seki Y, Kawamura H, Tochio D (2005) DNS of turbulent channel flow at very low Reynolds numbers. In: 4th international symposium on turbulence and shear flow phenomena, 1406.0248
- Uberoi MS (1956) Effect of wind-tunnel contraction on free-stream turbulence. *J Aeronaut Sci.* <https://doi.org/10.2514/8.3651>
- Vasudevan B, Prabhu A, Narasimha R (1992) Blade manipulators in turbulent channel flow. *Exp Fluids.* <https://doi.org/10.1007/BF00188259>
- Whan GA, Rothfus RR (1959) Characteristics of transition flow between parallel plates. *AIChE J.* <https://doi.org/10.1002/aic.690050215>
- White FM (1991) *Viscous fluid flow*, 2nd edn. McGraw Hill, New York
- Wynanski IJ, Champagne FH (1973) On transition in a pipe. Part 1. The origin of puffs and slugs and the flow in a turbulent slug. *J Fluid Mech.* <https://doi.org/10.1017/S0022112073001576>
- Zanoun ESM (2003) Answers to some open questions in wall bounded laminar and turbulent shear flows. Ph.D. thesis, Universität Erlangen-Nürnberg, Erlangen

**Publisher's Note** Springer Nature remains neutral with regard to jurisdictional claims in published maps and institutional affiliations.